Equation (55) for G in closed form behaves as described in the text. It reduces to unity for $\eta=0$, and with increasingly large η it generates sharp maxima at integral h_1 and h_2.

References

BAGARYATSKII, A., NOSOVA, G. J. & TAGUNOVA, T. V. (1955). *Dokl. Akad. Nauk. SSSR*, **105**, 1225–1228.

KEATING, D. T., AXE, J. D. & MOSS, S. C. (1973). In preparation.

SASS, S. L. (1972). *J. Less. Common Metals*, **28**, 157–173.

SASS, S. L. & BORIE, B. (1972). *J. Appl. Cryst.* **5**, 236–238.

SILCOCK, J. M., DAVIES, M. H. & HARDY, H. K. (1955). *Symposium on the Mechanism of Phase Transformations in Metals*, pp. 93–104. London: Institute of Metals.

YAKEL, H. L. (1972). Private communication.

Acta Cryst. (1973). A**29**, 594

The Short-Range Structure of Ti and Zr B.C.C. Solid Solutions Containing the ω Phase. II. Solution of the Structure Determination*

BY BERNARD BORIE,† STEPHEN L. SASS & ALF ANDREASSEN‡

Department of Materials Science and Engineering, Cornell University, Ithaca, New York 14850, *U.S.A.*

(*Received* 14 *December* 1972; *accepted* 11 *April* 1973)

Our new techniques for computing intensity distributions from atomic arrangements with defects in periodicity were applied to a variety of models in an attempt to reproduce in detail the diffuse neutron-diffraction pattern of a Zr–20 wt.% Nb alloy quenched from 1273°K. The model which succeeds is described, and its kinematic intensity sum is derived. The resultant computed diffuse intensity distribution is compared with experiment.

Introduction

In a companion paper (Borie, Sass & Andreassen, 1973, referred to here as Part I), the calculation of diffuse intensity distributions in reciprocal space resulting from the formation of the ω phase in b.c.c. solid solutions was described. The theory correctly separates the diffraction pattern into two parts: sharp fundamental Bragg maxima (those common both to b.c.c. and ω); and superstructure reflections, the details of which depend on the model used to specify the atomic positions. For a simple model, broadened superstructure maxima, forming planes of diffuse intensity whose normal is **c*** (the hexagonal basis vector of the reciprocal unit cell of the ω phase) were found. Though this result is qualitatively compatible with experiment, the model failed to reproduce the details of the observed intensity distribution. Specifically, superstructure peak shifts parallel to **c*** were found which are opposite in direction to those observed. Though relative intensities of the superstructure maxima derived from the model agreed qualitatively with experiment, a quantitative fit was not attempted.

* Research sponsored by the U. S. Atomic Energy Commission under contract with the Union Carbide Corporation, the Metallurgy Branch of the U. S. Office of Naval Research, and the U. S. Air Force.

† Also at the Metals and Ceramics Division, Oak Ridge National Laboratory, Oak Ridge, Tennessee 37830, U.S.A.

‡ Present Address: The Applied Physics Laboratory of Johns Hopkins University, Howard County Facility, 8623 Georgia Avenue, Silver Spring, Maryland 20910.

The model tested in Part I was that of a crystal composed of regions of either untransformed b.c.c. (the β phase), or wholly transformed ω, containing no fragments of ω cells. Diffuse effects and peak shifts were taken to result from anomalous interference effects among the subvariants of the system, as illustrated in Fig. 1, Part I.

The result of our calculation displayed in Figs. 3 and 4 of Part I is valid only for the special composition $\frac{1}{4}\beta$, $\frac{3}{4}\omega$ (by volume), and for a random distribution of integral ω cells and β translational entities in columns parallel to **c***. Its generalization to arbitrary composition and states of order failed to reverse the peak shifts.

We conclude from this that the crystal probably contains local atomic configurations not found in either ω or β regions. If that be the case, the diffraction pattern provides few clues as to what such a configuration may be. At this point in our understanding of the solution of short-range structure problems, we are reduced to testing physically plausible models.

We describe here the last in a series of models, which reproduces quantitatively the observed diffraction pattern. The diffuse intensity distribution to be fit by theory was taken to be that of Keating, Axe & Moss (1973) shown in Fig. 1. Since it was measured with neutrons, it is relatively free of the double diffraction and dynamical effects which plague electron-diffraction patterns, and it is free of form factor effects which cause X-ray measurements to be of uneven statistical quality.

The contour map of Fig. 1 is the intensity distribution in the plane $k=0$ at 300°K for a Zr–20 wt.% Nb

alloy quenched from 1273°K. The diffuse intensity was found to be elastic, indicating that the deviations from periodicity in the alloy are of static rather than elastic origin. The hexagonal coordinate system shown is relevant to one of the four variants of the system, with integer values of the continuous variables h_1H_3 corresponding to the Miller indices. The diagonal tails appended to the right of the 002, 103 and 201 diffuse maxima are associated with the second variant whose c^* axis also lies in the plane of measurement and are omitted from consideration in what follows. As in Part I, we assume that the variants of system scatter independently.

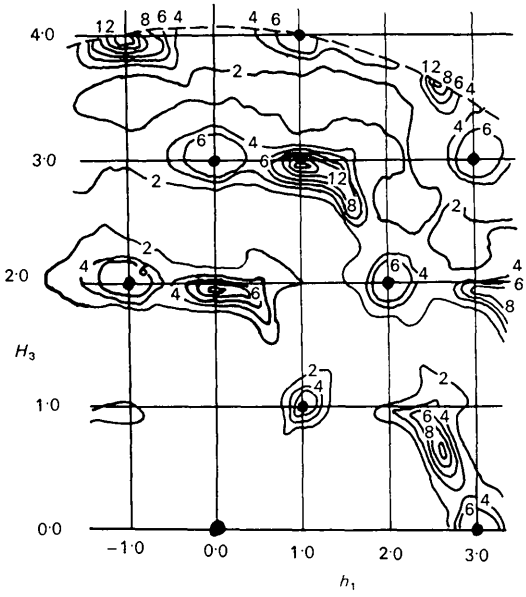

Fig. 1. Contour map of the diffuse neutron intensity distribution in the $h_1 0 H_3$ plane of reciprocal space at 300°K for Zr–20 wt.% Nb quenched from 1273°K.

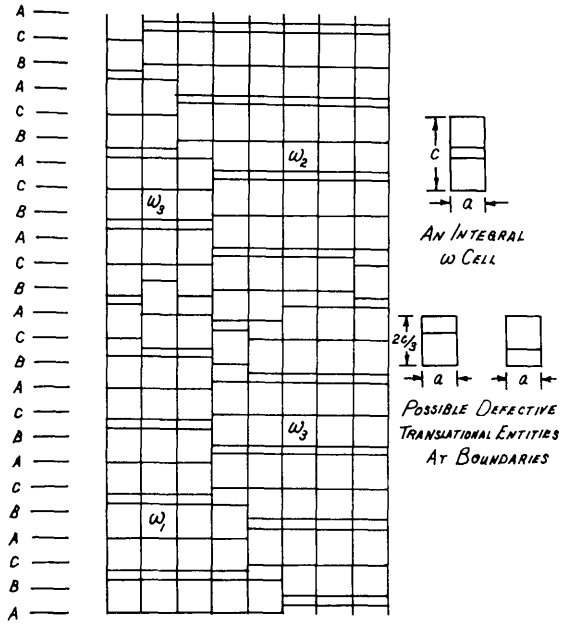

Fig. 2. Schematic illustration of the three subvariants of the system with defective translational entities at the subvariant boundaries.

Description of the model

For simplicity we take the crystal to be completely transformed, containing no b.c.c. regions. We adopt the convention established in Fig. 1, Part I: After having labeled the hexagonal planes A, B, or C according to the stacking sequence, we identify an ω region as subvariant one if the plane undisplaced on transformation is an A plane. It is subvariant two if the undisplaced plane is B, and three if it is C. Fig. 2 illustrates the way in which we presume space to be filled with the three subvariants. An important detail of the model is the assumed nature of the boundary regions in vertical columns of cells parallel to **c**. Transitions between subvariants in such columns are to be allowed only *via* the two defective translational entities shown in the Figure. Note that the atomic environment in such a defect is different from that of either the ω or the β phase. Because the defective region has a dimension parallel to **c** of $2c/3$, it follows that in vertical columns of cells, the model requires that ω_1 be followed by ω_3 and never by ω_2. In a vertical column, we require that a defective translational entity be both preceded and followed by an integral ω cell. We take the crystal to be a three-dimensional mosaic constructed of integral ω cells and the defective entities shown.

Let v_1 and v_2 specify the two defective configurations, and let γ be the probability that in a vertical column an ω cell is followed by either of them. Then the probability of finding the configuration $\omega v_1 \omega$ (or $\omega v_2 \omega$) is $\gamma/2$. The average number of ω cells between faults in a column is $1/\gamma$. Hence for $1/\gamma$ cells of ω, there are $\frac{1}{2}v_1$ configurations and $\frac{1}{2}v_2$. Because an ω cell has a volume which is $\frac{3}{2}$ that of a defective translational entity, the volume fraction of the crystal that is v_1 (or v_2) is

$$x = \tfrac{1}{2}\left\{1/\left(1+\frac{3}{2\gamma}\right)\right\} = \gamma/(2\gamma+3)\,. \qquad (1)$$

The volume fraction of the crystal composed of integral cells associated with, say, subvariant one is

$$y = \tfrac{1}{3}(1-2x) = 1/(2\gamma+3)\,. \qquad (2)$$

Diffraction theory

We choose an atom in the crystal at random and examine its environment. If transformation has left it undisplaced, it may be preceded by an ω cell or by either of the defective configurations. This is illustrated schematically by the first three elements shown in Fig. 3. If it is displaced downward it may either be in an ω_2 region or in one of the defective configurations as represented by the next two elements of the Figure. Its environment for an upward displacement is shown in the final two elements of the Figure.

Having specified the environment of the origin, we proceed to translate a distance $n_1\mathbf{a}_1+n_2\mathbf{a}_2$. As in Part I, we choose to characterize the result of that translation in terms of p, the number of boundaries crossed in the course of the translation.

We may use the probabilities P_p and P_p' as defined and derived in Appendix A, Part I, for T 'different' regions in the hexagonal plane. The condition that the regions be different used in the derivation is not formally necessary and was used for the sake of clarity. We may set S of them to be identical and to correspond to, say, ω_1 regions. Then S is determined by the requirement that $S/T=y$ as given by equation (2). We obtain

$$S/T=1(2\gamma+3)\,. \tag{3}$$

Equation (3) may be interpreted as the probability that as we sample various parts of a hexagonal plane we find the plane corresponding to an ω_1 (or ω_2 or ω_3) region, in the sense of Fig. 3. The number of regions in the plane associated with defective configurations is $T-3S$. Hence, as we sample the plane, the probability that it corresponds to one of the four defective regions represented by elements two, three, five, and seven of Fig. 3 is $\frac{1}{4}(1-3S/T)=\frac{1}{2}x$; or with equation (1),

$$\tfrac{1}{4}(1-3S/T)=\gamma/(4\gamma+6)\,. \tag{4}$$

Using the notation of Part I, we wish to compute $\langle\exp[2\pi i(\kappa_n-\kappa_0)h_3]\rangle$ for our model and to substitute the result into equation (7), Part I, to obtain the intensity distribution in reciprocal space. To that end, we define probabilities ${}_0\sigma_n$, ${}_+\sigma_n$, and ${}_-\sigma_n$ having to do with the arrangement of translational entities in a vertical column parallel to $\mathbf{c}$. ${}_0\sigma_n$ is the probability that, beginning with an undisplaced atom preceded by an integral ω cell, we traverse n hexagonal planes and find that atom undisplaced. ${}_+\sigma_n$ is the probability that the nth such atom is displaced upward and ${}_-\sigma_n$ the probability that it is displaced downward.

We may now write the contribution to $\langle\exp[2\pi i(\kappa_n-\kappa_0)h_3]\rangle$ for those $n_1n_2n_3$ atomic pairs which begin with the origin in an ω_1 region:

$$\begin{aligned}\langle\exp[2\pi i(\kappa_n-\kappa_0)h_3]\rangle_1=&\frac{S}{T}P_p\{{}_0\sigma_{n_3}+{}_+\sigma_{n_3}\exp[2\pi ih_3]\\&+{}_-\sigma_{n_3}\exp[-2\pi ih_3]\}+\frac{S}{T}P_p'(S-1)\{{}_0\sigma_{n_3}\\&+{}_+\sigma_{n_3}\exp[2\pi ih_3]+{}_-\sigma_{n_3}\exp[-2\pi ih_3]\}\\&+\frac{S}{T}P_p'S\{{}_0\sigma_{n_3-1}+{}_+\sigma_{n_3-1}\exp[2\pi ih_3]\\&+{}_-\sigma_{n_3-1}\exp[-2\pi ih_3]\}+\frac{S}{T}P_p'S\{{}_0\sigma_{n_3-2}\\&+{}_+\sigma_{n_3-2}\exp[2\pi ih_3]+{}_-\sigma_{n_3-2}\exp[-2\pi ih_3]\}\\&+\frac{S}{T}P_p'\tfrac{1}{2}(T-3S)\{{}_0\sigma_{n_3-3}+{}_+\sigma_{n_3-3}\exp[2\pi ih_3]\\&+{}_-\sigma_{n_3-3}\exp[-2\pi ih_3]\}+\frac{S}{T}P_p'\tfrac{1}{2}(T-3S)\{{}_0\sigma_{n_3-4}\\&+{}_+\sigma_{n_3-4}\exp[2\pi ih_3]+{}_-\sigma_{n_3-4}\exp[-2\pi ih_3]\}\,.\end{aligned} \tag{5}$$

In equation (5), S/T is the probability that the origin is in an ω_1 region. $(S/T)P_p$ is the probability that we begin in such a region, traverse p boundaries in the hexagonal plane, and find ourselves in an identical region. The coefficient of $(S/T)P_p$ is the result of a vertical translation n_3 in terms of the σ_{n_3}'s, beginning with an undisplaced atom at $n_3=0$.

$(S/T)P_p'$ is the probability that after the translation, we find ourselves in a region 'different' from the origin. But since we have taken S of the T 'different' regions to provide identical environments, the coefficient of $(S/T)P_p'(S-1)$ must be the same as that of $(S/T)P_p$.

If we begin the translation n_3 in ω_2, the atom at $n_3=1$ must be undisplaced, as shown in Fig. 3. Hence the subscripts on the σ_{n_3}'s in the coefficient of the first $(S/T)P_p'S$ are reduced by one. Those on the σ_{n_3}'s in the coefficient of the second $(S/T)P_p'S$ in equation (5) are reduced by two, corresponding to beginning n_3 in ω_3.

The probability that the hexagonal translation terminates in the defective configurations shown by the second and third elements of Fig. 3 is $(S/T)P_p'\frac{1}{2}(T-3S)$. Here, though the plane at $n_3=0$ is undisplaced, we have required that these configurations always be followed by at least one integral ω cell. Hence the atom at $n_3=3$ must be undisplaced, and the subscripts on the σ_{n_3}'s must be reduced by three for the n_3 translation. Similarly, for hexagonal translations terminating in regions represented by the fifth and seventh elements of Fig. 3, the subscripts must be reduced by four.

With expressions (41) and (42), Appendix A, Part I, substitute for P_p and P_p' in equation (5). After some rearrangement there results

$$\begin{aligned}\langle\exp[2\pi i(\kappa_n-\kappa_0)h_3]\rangle_1=&\frac{S}{T}\Big\{\frac{S}{T}([{}_0\sigma_{n_3}+{}_0\sigma_{n_3-1}\\&+{}_0\sigma_{n_3-2}]+[{}_+\sigma_{n_3}+{}_+\sigma_{n_3-1}+{}_+\sigma_{n_3-2}]\exp[2\pi ih_3]\\&+[{}_-\sigma_{n_3}+{}_-\sigma_{n_3-1}+{}_-\sigma_{n_3-2}]\exp[-2\pi ih_3])\\&+\tfrac{1}{2}(1-3S/T)([{}_0\sigma_{n_3-3}+{}_0\sigma_{n_3-4}]\\&+[{}_+\sigma_{n_3-3}+{}_+\sigma_{n_3-4}]\exp[2\pi ih_3]\\&+[{}_-\sigma_{n_3-3}+{}_-\sigma_{n_3-4}]\exp[-2\pi ih_3])\Big\}\left[1-\left(-\frac{1}{T-1}\right)^p\right]\\&+\frac{S}{T}\left(-\frac{1}{T-1}\right)^p({}_0\sigma_{n_3}+{}_+\sigma_{n_3}\exp[2\pi ih_3]\\&+{}_-\sigma_{n_3}\exp[-2\pi ih_3])\,.\end{aligned} \tag{6}$$

Consider the quantity in equation (6) in curly brackets, called $\mathscr{F}_{n_3}$. Upon elimination of S/T with equation (3) it becomes

$$\begin{aligned}\mathscr{F}_{n_3}=&\frac{1}{2\gamma+3}\{[{}_0\sigma_{n_3}+{}_0\sigma_{n_3-1}+{}_0\sigma_{n_3-2}\\&+\gamma({}_0\sigma_{n_3-3}+{}_0\sigma_{n_3-4})]+[{}_+\sigma_{n_3}+{}_+\sigma_{n_3-1}+{}_+\sigma_{n_3-2}\\&+\gamma({}_+\sigma_{n_3-3}+{}_+\sigma_{n_3-4})]\exp[2\pi ih_3]+[{}_-\sigma_{n_3}+{}_-\sigma_{n_3-1}\\&+{}_-\sigma_{n_3-2}+\gamma({}_-\sigma_{n_3-3}+{}_-\sigma_{n_3-4})]\exp[-2\pi ih_3]\}\,.\end{aligned} \tag{7}$$

For σ_n's all of the same prefix, there exists a relation. Beginning with the origin, with probability $1-\gamma$, we may have an integral ω cell, or, with probability γ, we may have a defective configuration followed by an ω cell. Hence for any n

$$\sigma_n=(1-\gamma)\sigma_{n-3}+\gamma\sigma_{n-5}\,. \tag{8}$$

Elimination of ${}_0\sigma_{n_3}$, ${}_+\sigma_{n_3}$, and ${}_-\sigma_{n_3}$ from equation (7) with (8) yields

$$\begin{aligned}\mathscr{F}_{n_3}=&\frac{1}{2\gamma+3}\{[{}_0\sigma_{n_3-1}+{}_0\sigma_{n_3-2}+{}_0\sigma_{n_3-3}\\&+\gamma({}_0\sigma_{n_3-4}+{}_0\sigma_{n_3-5})]+[{}_+\sigma_{n_3-1}+{}_+\sigma_{n_3-2}+{}_+\sigma_{n_3-3}\\&+\gamma({}_+\sigma_{n_3-4}+{}_+\sigma_{n_3-5})]\exp[2\pi ih_3]+[{}_-\sigma_{n_3-1}+{}_-\sigma_{3n-2}\\&+{}_-\sigma_{n_3-3}+\gamma({}_-\sigma_{n_3-4}+{}_-\sigma_{n_3-5})]\exp[-2\pi ih_3]\}\\=&\mathscr{F}_{n_3-1}\,.\end{aligned} \tag{9}$$

Since equation (9) must hold for any n_3, $\mathscr{F}$ is invariant and independent of n_3. To find $\mathscr{F}$ we may enumerate the σ_n's for $n\le 4$ and substitute the result into equation (7):

$${}_0\sigma_0=1;\ {}_0\sigma_1=0;\ {}_0\sigma_2=\gamma;\ {}_0\sigma_3=1-\gamma;\ {}_0\sigma_4=0\,, \tag{10}$$

$${}_+\sigma_0=0;\ {}_+\sigma_1=1-\tfrac{1}{2}\gamma;\ {}_+\sigma_2=0;\ {}_+\sigma_3=\gamma;\quad {}_+\sigma_4=(1-\gamma)(1-\tfrac{1}{2}\gamma)\,, \tag{11}$$

$${}_-\sigma_0=0;\ {}_-\sigma_1=\tfrac{1}{2}\gamma;\ {}_-\sigma_2=1-\gamma;\ {}_-\sigma_3=0;\quad {}_-\sigma_4=\tfrac{1}{2}\gamma(3-\gamma)\,. \tag{12}$$

We obtain

$$\mathscr{F}=\frac{1}{2\gamma+3}\{(1+\gamma)+(1+\gamma/2)\exp[2\pi ih_3]+(1+\gamma/2)\exp[-2\pi ih_3]\}\,. \tag{13}$$

We may also obtain $\mathscr{F}$ by considering the limiting values approached by the σ_n's for large n. In that case the environment of the origin is not relevant, and the limit approached by ${}_0\sigma_n$ is simply the probability that an atom in a hexagonal plane is undisplaced. This limit is simply the sum of the probabilities associated with elements one, two, and three of Fig. 3. With the aid of equations (3) and (4) we find

$$\lim_{n\to\infty}{}_0\sigma_n=1/(2\gamma+3)+2[\gamma/(4\gamma+6)]=(1+\gamma)/(2\gamma+3)\,, \tag{14}$$

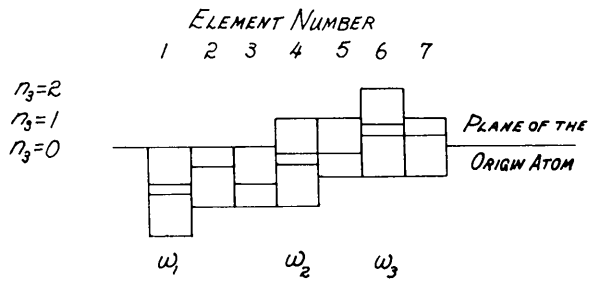

Fig. 3. Schematic illustration of the various possible atomic environments in a hexagonal plane.

while

$$\lim_{n\to\infty}{}_+\sigma_n=\lim_{n\to\infty}{}_-\sigma_n=1/(2\gamma+3)+\gamma/(4\gamma+6)=(1+\gamma/2)/(2\gamma+3)\,. \tag{15}$$

Substitution of the limiting values of the σ_n's into equation (7) or (9) gives equation (13). $\mathscr{F}$ has a meaning parallel to that of the analogous quantity developed in Part I: it is the average structure factor per atom.

With S/T eliminated from the remaining parts of equation (6) with (3) we obtain

$$\langle\exp[2\pi i(\kappa_n-\kappa_0)h_3]\rangle_1=\frac{1}{2\gamma+3}\left\{\mathscr{F}+\left(-\frac{1}{T-1}\right)^p({}_0\sigma_{n_3}+{}_+\sigma_{n_3}\exp[2\pi ih_3]+{}_-\sigma_{n_3}\exp[-2\pi ih_3]-\mathscr{F})\right\}. \tag{16}$$

Expressions similar to (16) may be developed for the contribution to the relevant average for those atomic pairs whose origins are found in ω_2 and ω_3 regions. Subscripts on the contributions refer to the relevant elements of Fig. 3.

$$\langle\exp[2\pi i(\kappa_n-\kappa_0)h_3]\rangle_4=\frac{\exp[2\pi ih_3]}{2\gamma+3}\left\{\mathscr{F}+\left(-\frac{1}{T-1}\right)^p({}_0\sigma_{n_3-1}+{}_+\sigma_{n_3-1}\exp[2\pi ih_3]+{}_-\sigma_{n_3-1}\exp[-2\pi ih_3]-\mathscr{F})\right\} \tag{17}$$

$$\langle\exp[2\pi i(\kappa_n-\kappa_0)h_3]\rangle_6=\frac{\exp[-2\pi ih_3]}{2\gamma+3}\left\{\mathscr{F}+\left(-\frac{1}{T-1}\right)^p({}_0\sigma_{n_3-2}+{}_+\sigma_{n_3-2}\exp[2\pi ih_3]+{}_-\sigma_{n_3-2}\exp[-2\pi ih_3]-\mathscr{F})\right\}. \tag{18}$$

For the four defective configurations of Fig. 3 we find

$$\langle\exp[2\pi i(\kappa_n-\kappa_0)h_3]\rangle_2+\langle\exp[2\pi i(\kappa_n-\kappa_0)h_3]\rangle_3=\frac{\gamma}{2\gamma+3}\left\{\mathscr{F}+\left(-\frac{1}{T-1}\right)^p({}_0\sigma_{n_3-3}+{}_+\sigma_{n_3-3}\exp[2\pi ih_3]+{}_-\sigma_{n_3-3}\exp[-2\pi ih_3]-\mathscr{F})\right\}; \tag{19}$$

$$\langle\exp[2\pi i(\kappa_n-\kappa_0)h_3]\rangle_5=\frac{\gamma\exp[2\pi ih_3]}{4\gamma+6}\left\{\mathscr{F}+\left(-\frac{1}{T-1}\right)^p({}_0\sigma_{n_3-4}+{}_+\sigma_{n_3-4}\exp[2\pi ih_3]+{}_-\sigma_{n_3-4}\exp[-2\pi ih_3]-\mathscr{F})\right\}; \tag{20}$$

$$\langle\exp[2\pi i(\kappa_n-\kappa_0)h_3]\rangle_7=\frac{\gamma\exp[-2\pi ih_3]}{4\gamma+6}\left\{\mathscr{F}+\left(-\frac{1}{T-1}\right)^p({}_0\sigma_{n_3-4}+{}_+\sigma_{n_3-4}\exp[2\pi ih_3]+{}_-\sigma_{n_3-4}\exp[-2\pi ih_3]-\mathscr{F})\right\}. \tag{21}$$

Equations (16) through (21) may be combined to give

$$\langle \exp[2\pi i(\kappa_n-\kappa_0)h_3]\rangle = \mathscr{F}^2 + \left(-\frac{1}{T-1}\right)^p \psi_{n_3}, \quad (22)$$

where

$$\psi_n = \frac{1}{2\gamma+3}\{[{}_0\sigma_n + {}_-\sigma_{n-1} + {}_+\sigma_{n-2} + \gamma_0\sigma_{n-3} + \tfrac{1}{2}\gamma_+\sigma_{n-4} + \tfrac{1}{2}\gamma_-\sigma_{n-4}] + [{}_+\sigma_n + {}_0\sigma_{n-1} + \gamma_+\sigma_{n-3} + \tfrac{1}{2}\gamma_0\sigma_{n-4}] \times \exp[2\pi i h_3] + [{}_-\sigma_n + {}_0\sigma_{n-2} + \gamma_-\sigma_{n-3} + \tfrac{1}{2}\gamma_0\sigma_{n-4}] \times \exp[-2\pi i h_3] + [{}_+\sigma_{n-1} + \tfrac{1}{2}\gamma_+\sigma_{n-4}] \exp[2\pi i 2h_3] + [{}_-\sigma_{n-2} + \tfrac{1}{2}\gamma_-\sigma_{n-4}] \exp[-2\pi i 2h_3]\} - \mathscr{F}^2. \quad (23)$$

Note that substitution of the limits given by equations (14) and (15) and $\mathscr{F}$ from equation (13) into (23) gives

$$\lim_{n\to\infty} \psi_n = 0. \quad (24)$$

Substitution of equation (22) into equation (7), Part I, leads as before to equation (20), Part I, except that the sum over p becomes $\sum_{p=0}^{n_1+n_2} S_p^{n_1+n_2}\left(-\frac{1}{T-1}\right)^p$.

The meaning of $S_p^{n_1+n_2}$ is unchanged. We have generalized the result of Part I for the special case of $T=4$ to arbitrary T. The meaning of α is as before, and the development leading to equations (21) through (25), Part I, follows, except that the definition of η is generalized:

$$\eta = 1-\alpha T/(T-1). \quad (25)$$

Appendix C, Part I, concerned with the evaluation of $G(h_1h_2)$, holds without change. The structural meaning of α and T, given that we have taken certain of the T regions to be identical, is discussed in the Appendix.

The summation giving the function $Q(h_1h_2h_3)$ may be found from equation (24), Part I (or, if the atomic displacements are taken to be $c/9$ rather than $c/6$, equation (37), Part I), taking ψ_n to be given by equation (23). The values of the σ_n's relevant to the computation of any ψ_n may be obtained using equation (8) as a recursion formula and the first four values of ${}_0\sigma_n$, ${}_+\sigma_n$, and ${}_-\sigma_n$ as given by equations (10), (11) and (12). Relations, of course, exist among the three kinds of σ_n's – for example, ${}_0\sigma_n + {}_+\sigma_n + {}_-\sigma_n = 1$ – so that equation (23) could be simplified. However, it is readily handled by a computer as given.

Because the smallest subscript on σ_n in equation (23) is $n-4$, the ψ_n's for $n<4$ must be treated as special cases, as in Part I. We find

$$\psi_0 = 1-\mathscr{F}^2; \quad (26)$$

$$\psi_1 = \frac{1}{2\gamma+3}\{(2+\gamma)\exp[2\pi i h_3] + \gamma\exp[-2\pi i h_3] + \exp[-2\pi i 2h_3]\} - \mathscr{F}^2, \quad (27)$$

$$\psi_2 = \frac{1}{2\gamma+3}\{2\gamma+2\exp[-2\pi i h_3] + \exp[2\pi i 2h_3]\} - \mathscr{F}^2, \quad (28)$$

$$\psi_3 = \frac{1}{2\gamma+3}\{3-\gamma+2\gamma\exp[2\pi i h_3] + \gamma\exp[-2\pi i 2h_3]\} - \mathscr{F}^2, \quad (29)$$

where $\mathscr{F}$ is as given by equation (13). The simple form of ψ_0, which was also found for the model used in Part I, is a general result.

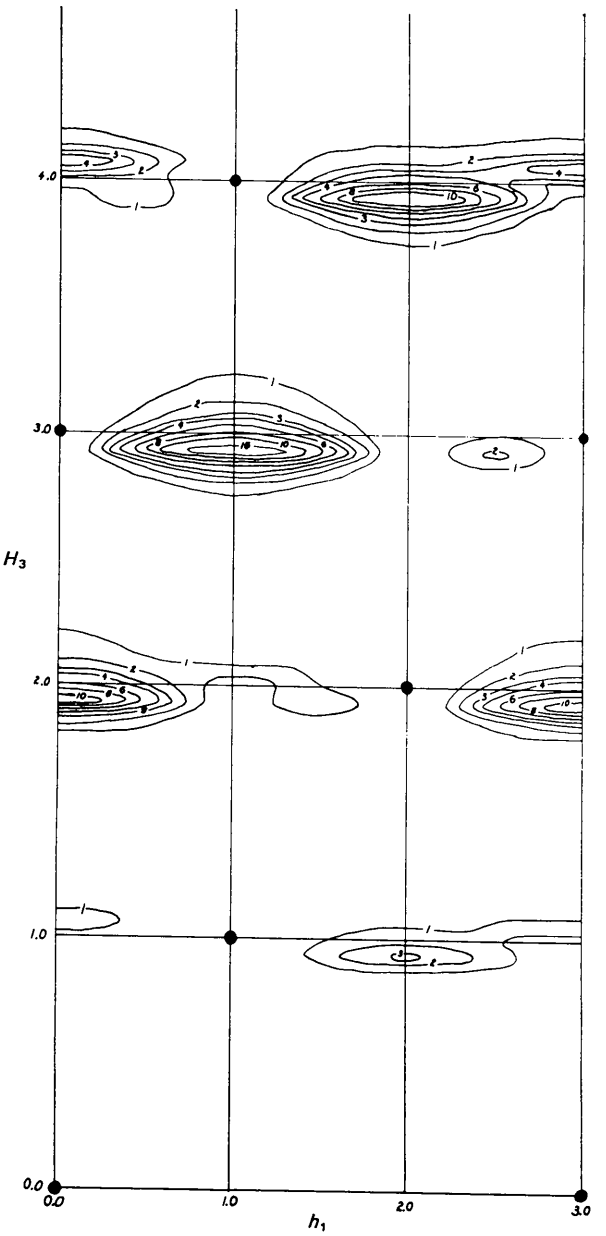

Fig. 4. The function $Q(h_10H_3)$ for Model I.

Results and discussion

Fig. 4 shows the function $Q(h_1OH_3)$ computed as described above. The atomic shifts were taken to be $c/9$, so the map was obtained with equation (37), Part I. The summation of that equation was terminated at $|n_3|=50$. The variable $H_3=9h_3$ as in Fig. 4, Part I. As before the point $(h_1, H_3)=(\frac{3}{2}, \frac{9}{2})$ is an inversion center, and the repeat intervals for the periodic function Q are $h_1=3$, $H_3=9$.

In contrast with the result of Part I, we have succeeded in reversing the directions of all of the peak shifts of the diffuse superstructure reflections, which now agree with those observed experimentally, as shown in Fig. 1. Our calculation has also resulted in fair agreement between observed and calculated relative intensities of the superstructure maxima, and it gives intensity distributions which are more extended laterally, as observed. Note that the diffuse maxima of Figs. 3 and 4, Part I, are much more nearly equiaxed than those of Figs. 1 and 4.

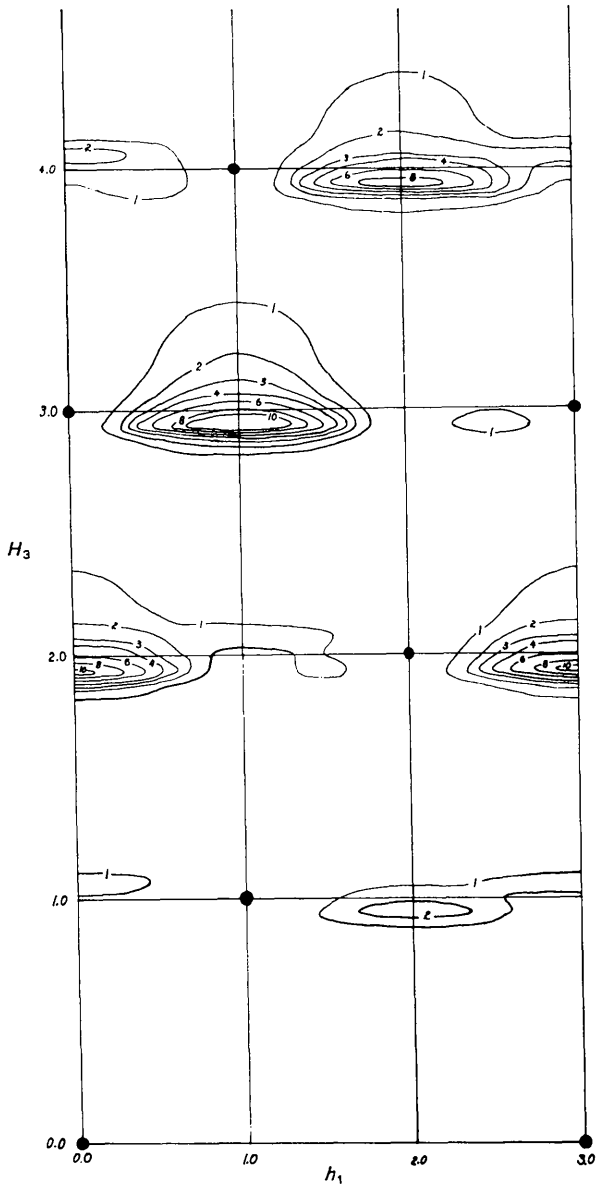

Fig. 5. The function $Q(h_1 0H_3)$ for Model II.

A value of $\gamma=0{\cdot}24$ was used for the calculation, which means that the average distance between faulted configurations in a vertical column is about $4c$. That value was chosen by monitoring the position of the 002 diffuse maximum as γ was varied, and taking that value which reproduced the shift measured by Keating, Axe & Moss (1973).

An inevitable ambiguity in structure problems is the question of uniqueness. In an effort to make some comment on that, we repeated our calculation for a slight variation of Model I, described above. Model II was taken to be identical to I, except that a single defective translational entity of height $2c/3$, with the central plane unshifted, was used. As before, this requires that in a vertical column ω_1 is always followed by ω_3. However the transition is accomplished by the insertion of an interval of height $2c/3$ of essentially untransformed β. Modification of the diffraction theory to accomodate this change is straightforward and will not be described.

Fig. 5 shows the resultant $Q(h_1OH_3)$ for Model II. The directions of the peak shifts are unaffected by the change, and remain correct. However, note that the strong diffuse maxima have become quite asymmetric, exhibiting pronounced high-angle tails, contrary to observation. Model II also causes poorer agreement with the observed relative intensities.

Table 1 is a quantitative comparison of relative peak intensities of the diffuse maxima generated by Models I and II with the measurements of Keating, Axe & Moss. Those *hkl*'s marked *F* are fundamentals and are not part of the diffuse-intensity distribution. The experimental values were read from Fig. 1 and normalized to unity for the strong 103 reflection. The entries in the Table for the two models were taken from Figs. 4 and 5 and similarly normalized. To complete the comparison, the square of the structure factor of the ω phase,

Table 1. *Comparison of diffuse peak intensities and the structure factor with experiment for Models* I *and* II ($u=\frac{1}{9}$)

hkl	Experiment	Model I	Model II	F^2/F^2_{103}
$\bar{1}01$	0·12	0·16	0·20	0·20
$\bar{1}02$	*F*	–	–	–
$\bar{1}03$	0·12	0·00	0·00	0·00
$\bar{1}04$	1·05	0·78	0·69	0·58
001	0·00	0·08	0·12	0·09
002	0·62	0·66	0·72	0·71
003	*F*	–	–	–
004	0·00	0·30	0·17	0·20
101	*F*	–	–	–
102	0·00	0·06	0·13	0·09
103	1·00	1·00	1·00	1·00
104	*F*	–	–	–

also normalized is included in the Table. The atomic positions used are those given in the introduction of Part I with $u=\frac{1}{9}$.

In all cases except $hkl=004$, Model II provides a poorer fit. Note also that the structure factor fails to reproduce the measured intensities. In fact, Keating, Axe & Moss comment that no value of u causes agreement between the square of the structure factor and their observations. Note that both models agree rather poorly with the measured intensity of the very strong $\bar{1}04$ reflection.

In an attempt to refine the agreement $Q(h_1OH_3)$ was computed for $u=\frac{1}{12}$, called Model III. In all other senses, Model III is identical to Model I. As was pointed out in Part I, such a change is easily incorporated into the calculation. We have that

$$Q(h_1h_2h_3)=\sum_{n_3}\psi_{n_3}\langle\exp[i\mathbf{k}\,.\,\boldsymbol{\delta}_{n_3}]\rangle\exp[8\pi i n_3h_3]\,. \quad (30)$$

Equation (30) is the analog of equations (24) and (37) of Part I, for an atom shift of $c/12$. The values of ψ_n used to obtain Q for Model I with equation (37), Part I, were used for Model III with equation (30).

Table 2 compares Model III and the structure factor squared for ω with $u=\frac{1}{12}$, with experiment. The entries in this table are normalized as in Table 1. Model III provides much improved agreement; we take it to be the solution to the structure.

Table 2. *Comparison of diffuse peak intensities and the structure factor with experiment for Model* III ($u=\frac{1}{12}$)

hkl	Experiment	Model III	F^2/F^2_{103}
$\bar{1}01$	0·12	0·10	0·13
$\bar{1}02$	*F*	–	–
$\bar{1}03$	0·12	0·05	0·07
$\bar{1}04$	1·05	0·97	1·21
001	0·00	0·08	0·07
002	0·62	0·66	0·53
003	*F*	–	–
004	0·00	0·01	0·00
101	*F*	–	–
102	0·00	0·10	0·13
103	1·00	1·00	1·00
104	*F*	–	–

Having chosen an appropriate Q, we may now find a value of η such that I_D/N, where

$$I_D/N=G(h_1h_2,\eta)Q(h_1h_2h_3,\gamma)\,, \quad (31)$$

with G given by equation (55), Appendix C, Part I, causes diffuse superstructure maxima whose lateral extension agrees with experiment. This was done by comparing the ratio of the peak intensity of the 002 reflection (Fig. 1) to that at the same value of H_3 but at $h_1=-\frac{1}{2}$, to the corresponding ratio from the computed Q. It was found that the ratios are very nearly the same, indicating that G must be very nearly structureless, or from equation (55), Part I, that η must be very nearly zero. A value of $\eta=0{\cdot}055$ caused best agreement. A contour map of I_D/N computed from equation (31) for Model III with $\gamma=0{\cdot}24$, $\eta=0{\cdot}055$ is shown in Fig. 6.

In addition to the contour map of Fig. 1, Keating, Axe & Moss measured a section through the center of the $\bar{2}03$ diffuse maxima (not shown on the Figure) parallel to H_3. Unlike the 103, which by our models must be its equivalent, it is unobscured by interference from a diffuse Bragg reflection from one of the other variants. With η and γ chosen to reproduce the peak intensities and the 002 shift, a further test of our model is its ability to match the shift and line contour of this reflection. Fig. 7 compares the measurements, made at 300 °K, with a section through the 103 reflection for Model III, Fig. 6. In both senses the agreement is good.

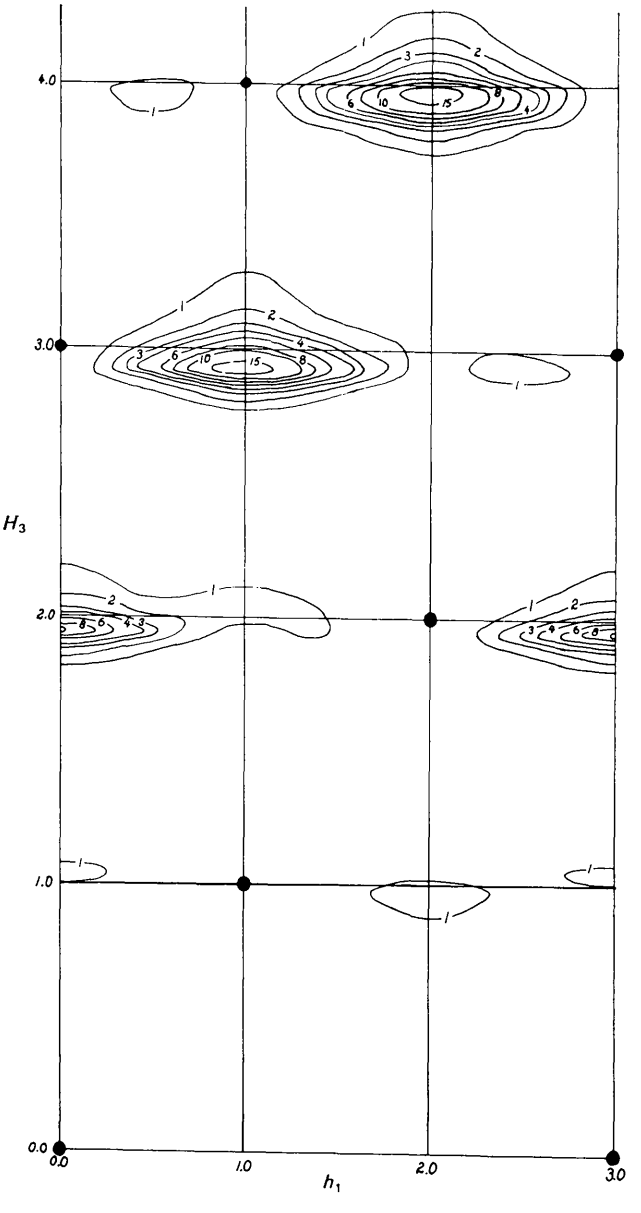

Fig. 6. The diffuse intensity, I_D/N, for Model III.

We comment briefly on some aspects of the meaning of our result. Our original concept described in Part I, that nuclei of ω associated with the three subvariants form at random and grow into each other, giving rise to interference effects which account for the diffraction pattern, must be incorrect. Under such circumstances ω_1 should be followed by ω_2 or ω_3 with equal probability, upon crossing a boundary in a vertical column. However, as we have seen, in order to reproduce the experimentally observed peak-shift directions, we have had to require that ω_1 be followed by ω_3. Other models with this property but incorrect in other senses also result in correct peak-shift directions, indicating that this correlation of the subvariant sequence with diffuse-maximum positions is a generalization. This result suggests that the diffraction effects are rather the result of growth faults, occurring as a single ω nucleus grows. The faults have a specific internal structure and occur with a rather high frequency as indicated by the observed value of γ.

A sense in which our model is artificially simple is that we have assumed that the crystal contains no untransformed β. We have presumed that the presence of regions of b.c.c. material should affect only the intensities of the fundamental maxima relative to the superstructure peaks, and not the relative details of the diffuse scattering alone. The development of a general diffraction theory for a partially transformed crystal awaits measurements of both components of the intensity distribution in absolute units. Any such theory must also include possible interference effects among the variants of the system. Such effects have been omitted in this treatment.

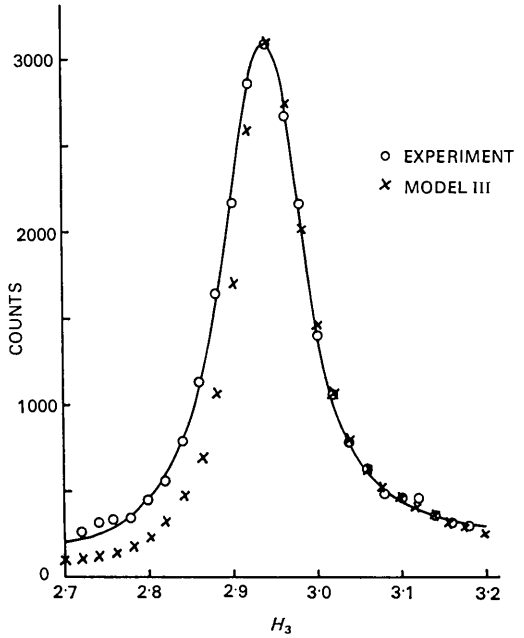

Fig. 7. Comparison of the measured intensity along the line $2\theta H_3$ for Zr-20 wt.% Nb quenched from 1273°K with Model III. The calculated points were scaled.

The authors are indebted to Drs David Keating, John Axe, and Simon Moss for permission to use their results. Discussions with Keating and Moss, and with Dr Harry Yakel and Mr Albert Chang were stimulating and useful.

APPENDIX

The average number of atoms in ω and defective regions in the hexagonal plane

In order to accomodate the statistics for translations in the hexagonal plane to a crystal composed of arbitrary relative numbers of integral cells and defective configurations, we took the plane to be divided into small regions in such a way that we could identify T 'different' regions. We let α be the probability that in a translation of $\mathbf{a}_1$, we crossed a boundary between two of the regions, the distribution of boundaries in the plane being random.

Choose an atom and require that it be preceded on the left by a boundary. Let $W(n)$ be the probability that we then translate $n\mathbf{a}_1$ to the right and encounter a boundary only on the last step. Then

$$W(n)=(1-\alpha)^{n-1}\alpha\,.$$

$W(n)$ is the probability of finding a row of n atoms between boundaries. Then the average number of atoms in such a row is

$$\langle n\rangle=\sum_{n=1}^{\infty}nW(n)=\alpha\sum_{n=1}^{\infty}n(1-\alpha)^{n-1}$$
$$=\alpha\frac{\mathrm{d}}{\mathrm{d}(1-\alpha)}\sum_{n=1}^{\infty}(1-\alpha)^n=1/\alpha\,.$$

Since the average number of rows in a region is $1/\alpha$ also, the average number of atoms in a region is $1/\alpha^2$.

We now set S of the T kinds of regions to be identical and to be ω_1 in the sense of element 1, Fig. 3. Similarly S regions correspond to ω_2 and S to ω_3, so that $\frac{1}{4}(T-3S)$ are to be associated with each of the defective configurations of Fig. 3.

Suppose we begin with an atom in one of the S regions which are ω_1. Then of the $T-1$ possible boundaries we may cross, $S-1$ of them are fictitous, $2S$ of them are ω_1/ω_2 or ω_3 boundaries, and $T-3S$ of them are ω_1/defect boundaries. Hence the probability that a boundary is real is

$$J=(2S+T-3S)/(T-1)=(T-S)/(T-1)\,.$$

Let m be the number of atoms in a row between real boundaries. Then

$$\langle m\rangle=\langle n\rangle J+2\langle n\rangle(1-J)J+\ldots$$
$$+m\langle n\rangle(1-J)^{m-1}J+\ldots$$

or

$$\langle m\rangle=\langle n\rangle J\sum_{m=1}^{\infty}m(1-J)^{m-1}=\langle n\rangle/J=1/\alpha(T-1)/(T-S)$$

and the average number of atoms in any of the three ω regions is

$$M_\omega = \frac{1}{\alpha^2}(T-1)^2/(T-S)^2 . \quad (32)$$

If we begin with an atom in one of the $\frac{1}{4}(T-3S)$ defective configurations, of the $T-1$ possible boundaries there are $\frac{1}{4}(T-3S)-1$ fictitous boundaries, $3(T-3S)/4$ defect/defect boundaries, and $3S$ defect/ω boundaries. Hence the probability that a boundary is real is

$$[3(T-3S)/4+3S]/(T-1)=\tfrac{1}{4}(T+S)/(T-1)$$

and the average number of atoms in any of the four defective regions is

$$M_D = \frac{16}{9\alpha^2}(T-1)^2/(T+S)^2 . \quad (33)$$

Equations (32) and (33) relate M_ω and M_D to α, T, and S, quantities which are essentially fictitous and not observable. We prefer to express them in terms of the experimentally measurable η and γ. With the aid of equations (3) and (25) we find that

$$M_\omega = \tfrac{1}{4}(2\gamma+3)^2/[(\gamma+1)^2(1-\eta)^2] , \quad (34)$$

and

$$M_D = \tfrac{4}{9}(2\gamma+3)^2/[(\gamma+2)^2(1-\eta)^2] . \quad (35)$$

A complete statistical description of the structure of the hexagonal plane should include not only the average sizes of the various regions, but as well the relative numbers of regions to be found in the plane. Consider a plane containing M atoms. Let there be V regions which are ω_1. If we choose an atom at random, the probability that it is in an ω_1 region is

$$\frac{VM_\omega}{M} = \frac{S}{T} = 1/(2\gamma+3)$$

by equation (3). So with equation (34), the number of ω_1 regions per atom in the plane is

$$\frac{V}{M} = \frac{4(\gamma+1)^2(1-\eta)^2}{(2\gamma+3)^3} . \quad (36)$$

Let there be W regions associated with one of the four possible defective configurations of Fig. 3 in the plane of M atoms. Then

$$M = 3VM_\omega + 4WM_D$$

and from equations (34), (35), and (36) the number of defective regions of a particular type per atom in the plane is

$$\frac{W}{M} = \tfrac{9}{8}\frac{\gamma(\gamma+2)^2(1-\eta)^2}{(2\gamma+3)^3} . \quad (37)$$

This means that though the average size of a defect region in the plane is a relatively insensitive function of γ [equation (35)], their number density in the plane decreases rapidly as γ becomes small.

With the values of $\gamma=0{\cdot}24$ and $\eta=0{\cdot}055$ found from the measurements, from equations (34) and (36), for any one of the three kinds of ω regions, there are on the average 2·20 atoms per region and 0·130 regions per atom in the plane. From equations (35) and (37), for one of the four kinds of defect regions, there are 1·20 atoms per region and 0·029 regions per atom in the plane. The hexagonal planes are very imperfect.

References

BORIE, B., SASS, S. L. & ANDREASSEN, A. (1973). *Acta Cryst.* A**29**, 585–594.

KEATING, D. T., AXE, J. D. & MOSS, S. C. (1973). In preparation.

Acta Cryst. (1973). A**29**, 602

On the Dependence of X-ray Debye–Waller Parameters on Atomic Form Factors

BY ROBERT F. STEWART*

Department of Physics, University of Western Australia, Nedlands, W. A. 6009, *Australia*

(*Received* 17 *November* 1972; *accepted* 21 *March* 1973)

An analysis of powdered-diamond diffraction data with Hartree–Fock and standard molecular C atomic form factors yields the Debye–Waller parameters $0{\cdot}20\pm0{\cdot}01$ and $0{\cdot}172\pm0{\cdot}009$ Å^2 respectively. The lattice-dynamic value, which is calculated here from published phonon dispersion curves measured by inelastic neutron scattering, is 0·149–0·150 Å^2 at 298°K. It is shown that a small amount of an orbital product, $\chi_{1s}^{SCF}\chi_{2s}^{STO}$, in the core atomic scattering factor can dramatically alter the Debye–Waller parameter. For diamond, this latter scattering factor gives a value of $0{\cdot}134\pm0{\cdot}009$ Å^2.

The determination of an accurate Debye–Waller factor for simple monatomic crystals by absolute X-ray diffraction intensities is generally limited by the model for crystal diffraction. In particular, thermal diffuse scattering and extinction phenomena make it difficult to infer true Bragg structure factors from a set of accurately measured intensities of X-ray scattering. Even if these difficulties can be successfully overcome, the analysis for the Debye–Waller factor at a single tem-

* Alfred P. Sloan Fellow. Present address: Department of Chemistry, Carnegie-Mellon University, 4400 Fifth Avenue, Pittsburgh, Pennsylvania 15213, U.S.A.